13 March 2026

A kinetic study of the crystallisation of LTA-type zeolite from colloidal solutions by in-situ ultrasonic attenuation measurement

Hasan Baser[1], Martin Hartmann[2], Wilhelm Schwieger[1,2]

1. Institute of Chemical Reaction Engineering, Friedrich-Alexander-Universität Erlangen-Nürnberg

2. Erlangen Center for Interface Research and Catalysis (ECRC)

Abstract

In the present study, we report the successful use of an ultrasonic device as a real-time, in-situ diagnostic tool for monitoring the crystallization progress of zeolite A from homogeneous, colloidal solutions with the composition 0.4 Na2O : 10 SiO2 : 1.4 Al2O3 : 16 (TMA)2O: X H2O (X: 650, 750, 850, 950, 1050). Kinetic information like reaction rate or reaction order of crystal growth can easily be calculated from the measured ultrasonic signal data. For the mathematical description of the crystallization curves, the experimental curves were fitted with different kinetic models. The crystallization proceeds in more than one step suggesting a change of the kinetics during the formation of the crystalline material. The evaluated reaction exponents for the different steps could only be described with the Avrami-Erofeyev nucleation model. The results indicate that-depending on amount of water in the synthesis mixture-first a three-dimensional and then a one-dimensional crystal growth takes place.

Keywords

Kinetic, in-situ, ultrasonic attenuation, colloidal synthesis, LTA, model descriptions

A kinetic study of the crystallisation of LTA-type zeolite from colloidal solutions by in-situ ultrasonic attenuation measurement

Hasan Baser[1], Martin Hartmann[2], Wilhelm Schwieger[1,2*]*

[1)] Friedrich-Alexander-Universität Erlangen-Nürnberg, Institute of Chemical Reaction Engineering, Egerlandstraße 3, 91058 Erlangen Germany

[2)] Friedrich-Alexander-Universität Erlangen-Nürnberg, Catalysis and Sustainable Processes, Erlangen Center for Interface Research and Catalysis (ECRC), Egerlandstraße 3, 91058 Erlangen, Germany

Abstract

In the present study, we report the successful use of an ultrasonic device as a real-time, in-situ diagnostic tool for monitoring the crystallization progress of zeolite A from homogeneous, colloidal solutions with the composition 0.4 Na_2O : 10 SiO_2 : 1.4 Al_2O_3 : 16 $(TMA)_2O$: X H_2O (X: 650, 750, 850, 950, 1050). Kinetic information like reaction rate or reaction order of crystal growth can easily be calculated from the measured ultrasonic signal data. For the mathematical description of the crystallization curves, the experimental curves were fitted with different kinetic models. The crystallization proceeds in more than one step suggesting a change of the kinetics during the formation of the crystalline material. The evaluated reaction exponents for the different steps could only be described with the Avrami-Erofeyev nucleation model. The results indicate that - depending on amount of water in the synthesis mixture - first a three-dimensional and then a one-dimensional crystal growth takes place.

Keywords: Kinetic, in-situ, ultrasonic attenuation, colloidal synthesis, LTA, model descriptions

Introduction

A better understanding of the mechanisms of zeolite formation and an improved control of the crystallization process are necessary to tailor the properties of zeolites meeting the ever-growing demand of their performance in various, sometimes very different, applications. In the past

decade, significant advances have been made in in-situ monitoring of the zeolite crystallization process. Such studies contributed considerably to the understanding of zeolite formation and enabled the identification of intermediate phases, which are usually thermodynamically unstable during the progress of zeolite crystallization. Several analytical techniques are currently in use for in-situ monitoring of the nucleation and growth process of different zeolite types [1-4], in particular Raman spectroscopies [4 - 6], NMR spectroscopy [7, 8] electron paramagnetic resonance [9], X-ray adsorption spectroscopy [10], X-ray/neutron diffraction [11,12], small- and wide-angle X-ray scattering [2,13,14], atomic force microscopy [15] and some others [16-22]. Most of the techniques reqiure a very high experimental and theoretical expenditure. Just few of them [16,17, 21] follow simple chemistry-based indicators like change in the viscosity and conductivity, however the interpretation of the resulting dependencies will be affected by just more than one effect.

In general, several mechanisms for the zeolite formation have been proposed based on the observations under specific synthesis conditions. However, no general mechanism was obtained to describe the formation of the zeolites in general because of the complexity of hydrothermal chemical reactions. Two main mechanisms for zeolite formation are proposed and generally accepted [1, 2, 4]: namely a) solution mediated transport mechanism and b) solid phase transformation mechanism.

Depending on the reaction conditions and the type of zeolite, crystallization can proceed after the first or the second mechanism. Examples for both can be found in a review article by Davis et al. [4]. It also happens that both mechanisms occur in the course of a single crystallization process. For the crystallization of zeolite A, both the solution mediated transport mechanism as well as the solid phase transformation mechanism were observed. Smaihi et al. have found that the crystallization process of LTA should be divided into two stages [24]. After formation of viable nuclei, a reorganization of the amorphous gel in the first stage of the crystal growth process takes place. By aggregating the nuclei, nanocrystals with a rough surface are formed. Similar aggregation observation was also reported by Mintova et al. [10]. In the second crystallization stage, a layer growth mechanism occurs, where transport of nutrients across the mother liquor takes place. As a consequence, "well-designed" zeolite crystals are obtained.

Cubillas et al. [25] have found that the surface property (rough or smooth) of the formed crystals is a function of the supersaturation of the mother liquor. For smaller supersaturations crystals with a smooth surface and at higher supersaturation crystals with a rough surface was observed [25]. A layer growth mechanism during the zeolite synthesis was also described by Agger et al. [26] using Atomic Force Microscopy.

However, compared to these methods ultrasonic monitoring is a non-destructive, cost-effective and robust technique based on the continuously measurement of ultrasonic attenuation and velocity in reaction fluid during the synthesis. In our previous studies, we have monitored the crystallization of zeolites A and X from dense and opaque synthesis gels [27-29]. The results demonstrated that a good correlation exists between the crystallization progress of zeolites and the ultrasonic attenuation and velocity. In our recent papers [30, 31], we have reported the successfull use of ultrasonic (US) meauserement to monitor of the crystallization progress and to derive of the kinetic data from ultrasonic attenuation measurements during the synthesis of Zeolite A and X extracted from alkaline fused coal fly ash.

For the production of zeolite A, nowadays syntheses from homogeneous solutions containing colloidal separated amorphous particles are carried out. Following this approach, colloidal suspension of zeolite A crystals with sizes below 100 nm and with a narrow particle size distribution can be obtained [10, 33] prior to the drastic growth of single crystals. Such suspensions are colloidally stable and the resulting, dispersed zeolite crystals do not settle down for longer period. Many studies to investigate the crystallization mechanism and kinetics were performed with such colloidal synthesis systems, in particular also for zeolite A [32-34].
Thus, to study this transformation we combined the two approaches (i) the use of the colloidal synthesis system with (ii) the in-situ measurement of the US measurement approach. As starting materials usually colloidal silica as silicon source and Al-isopropoxide ($[(CH_3)_2CHO]_3Al$) as aluminum source are used. Another important factor for the synthesis of nanosized crystals is the use of tertiary alkyl ammonium compounds as a template. They serve not only as a counter ion to compensate the negative charge of the forming framework, but also act as a structure directing agent to obtain the desired zeolite structure. Another advantage is that the templates are covering the surface of the nanocrystals formed and thereby prevent agglomeration of the crystals [35].

Thus in this paper, we follow the zeolite A crystallisation by continuous measurement of ultrasonic attenuation under real reaction conditions to generate high quality real sets of kinetic data allowing a better and detailed description of the crystallization process. By means of the application of different crystallization models and evaluations aspects, advantages and drawbacks of there use are discussed.

Description of the zeolite crystallization process

The usually S-shaped crystallization process of the zeolites can be described mathematically in different ways. Thus already in 1966, Kerr et al. suggested that the crystalline growth period of zeolite A can be described as an autocatalytic first-order kinetics [36]. Kerr starts from the generally accepted view that the active species of an amorphous gel can be rapidly transferred by a dissolution process into the solution and the speed of zeolite formation depends on the concentration of these active species in the solution. Thus, his model is based on the solution-mediated transport mechanism.

According to Kerr, the time dependence of the relative crystallinity (α) can be represented by the following exponential equation:

$$\alpha = \alpha_0 \, e^{kt} \tag{1}$$

or integrated:

$$\ln\alpha = \ln\alpha_0 \cdot kt \tag{2}$$

The parameter (k) can be regarded as an effective rate constant. (α_0) corresponds to the value of (α) at the time t=0, but has no physical significance if no zeolite seed crystals are present in the system at the beginning of crystallization.

Further simple equation for describing the zeolite A crystallization kinetic is based on a potency function of Ciric [37]:

$$\alpha = \mathrm{k} \cdot \mathrm{t}^{\mathrm{n}} \tag{3}$$

or integreted:

$$\ln\alpha = \ln(k) + n \cdot \ln(t) \tag{4}$$

Toufar [33] describes another approach. By fitting of the following model function to the measurement values of zeolite ZSM-5 crystallization employing a numerical iteration following the Marquadt method, he was able to reach a sufficient description of the crystallization process with only four parameters:

$$\alpha = \tfrac{1}{2} \cdot \left(\alpha_{\max} - k_R \cdot t_k\right) \cdot \left(1 + \tanh\left(k \cdot \left(t_k - t_l\right)\right)\right) \tag{5}$$

Here (α_{max}) is the highest values of the crystallinity, (k_R) the rate constant of the recrystallization, (k) the rate constant of the crystallization and (t_l) the sum of the time interval of the nucleation and the half-life of the crystal growth. In this case, the rate constant (k_R) regulates the gradient in the increase of the sigmoidal curve, (t_l) shifts the start of the crystal growth parallel on the time axis to the left or right. The Toufar model enables the calculation of the rate constant of recrystallization observed in zeolite syntheses after reaching the maximum crystallinity.

The previous models do not provide any information about the nucleation rate. The model of Avrami-Erofeyev was developed for the description of solid phase transformations and assumes that a solid phase transformation is driven by nucleation and subsequent growth [38, 39]. The reaction rate constant (k) contains the growth rate and nucleation rate.

$$\alpha = 1 - e^{-kt^n} \tag{6}$$

The linear relationship of the Avrami–Erofeyev equation is the so-called Sharp-Hancock [43] plot:

$$\ln(-\ln(1-\alpha)) = \ln(k) + n \cdot \ln(t - t_0) \tag{7}$$

In this equation (k) represents the reaction rate constant and (t), (α) and (n) the reaction time, the reaction progress and Avrami exponent (reaction order), respectively. The value (t_0) is the time for onset of crystallization. A plot ln(-ln(1-α)) versus ln(t-t_0) gives a straight line. The Avrami exponent (n) is obtained from the slope of the curve, whilst the reaction rate constant (k) can be evaluated from the intercept ln(k) with the y axis. Avrami equation in this form is widely used and here the Avrami exponent (n) is not taken into account when calculating the reaction rate constant [31, 36 – 40]. In some works the Avrami model was used in so-called ***modified*** form [31, 41-45]:

$$\alpha = 1 - e^{(-kt)^n} \tag{8}$$

or as Sharp-Hancock plot:

$$\ln(-\ln(1-\alpha)) = n \cdot \ln(k) + n \cdot \ln(t - t_0) \tag{9}$$

The difference between Avrami equation (6 and 7) and modified Avrami equation (8 and 9) is that the intercept of the ln(-ln(1-α)) vs ln(t-t_0) plot is ln(k) in the first (equation 7) and nln(k) in the second one (equation 9). Thus, in the modified Avrami equation the reaction rate constant (k) is a function of the Avrami exponent (n).

The so-called Avrami exponent (n) is a numerical exponent with values usually between 1 and 4. It is assumed that the value of the Avrami exponent depends on the dimensionality of the growth process similar to the reaction order in homogeneous kinetics.

Mandelkern [51] has modified the Avrami equation assuming that (i) the maximum achievable number of nuclei can result in different overall crystallisation rates, esp. when the process of the nuclei formation and the crystal growth are overlapping and that (ii) in spherical crystal growth of n-values of 3 to 4 (three-dimensional growth) and in a disk-shaped growth of 2 to 3 (two-dimensional growth). If the nucleation rate is very high, i.e. all nuclei are formed before appreciable crystallization has occurred, we obtain n = 3 (spherical growth) and n = 2 (disc-shaped growth). The nuclei are formed at a constant rate during the entire crystallization process (pure homogeneous nucleation), so n = 4 for spherical growth and n = 3 for disk-shaped growth. Accordingly, intermediate values are then obtained when the defined number of nuclei at a certain temperature is reached before the end of the crystallization. Values near 0.5 are expected when a reaction is diffusion-controlled. It also happens that a crystallization process consists of different mechanisms.

Gualtieri [52] used to describe the crystallization kinetics of zeolites with a model where nucleation and crystal growth are considered as separate processes:

$$\alpha = \frac{1}{1+\exp\left[-\left(\frac{t-a}{b}\right)\right]}\left(1-\exp\left[-(k_g t)^n\right]\right) \qquad (10)$$

The crystallization progress (α) is the same as in the Avrami model, (t) is the reaction time, (k_g) is the rate constant of crystal growth, (a) and (b) are constants related to nucleation. The inverse of (a) can be interpreted as the rate constant for nucleation ($k_n=a^{-1}$), whereas (b) provides information on the nucleation mechanism. The exponent (n) contains the information about the dimensionality of the crystal growth.

Eerlier, Culfaz and Sand [53] used *as* rate of crystallization simply the slope at the corresponding half-maximum crystallinity (α=0.5) on the crystallization curve (see Figure 11). The approximate rates of crystallization were calculated by taking the slopes of the crystallization curves at midway in the region where the yield was increasing.

Experimental Section

The following procedure was used to prepare the reaction mixture for the synhesis of the zeolite A crystals similar to our previous published procedure [54]. Synthesis solutions were prepared with colloidal silica (30% SiO_2 and 0.32% Na_2O; Ludox HS-30), aluminium isopropoxide (98%, (Al-$[(CH_3)_2CHO]_3$), sodium hydroxide (NaOH, 99%) and tetramethylammonium hydroxide (TMAOH, 25% aqueous). All chemicals were obtained from Aldrich. Solution A was prepared by dissolving 2.86 g of Al-$[(CH_3)_2CHO]_3$ and 4.0 g of NaOH (1M in H_2O) in 38.89 g TMAOH (25 wt % in H_2O). Deionized water (2.5 g) was then added into the solution A and stirred for 45 min. Solution B was prepared by mixing 19.45 g of TMAOH (25 wt % in H_2O), 10.00 g of Ludox HS-30 and 1.25 g of deionized water and stirred for 15 min. These two solutions (A and B) were mixed together and the mixed solution was stirred for 30 min. The molar composition of the resulting colloidal solution was:

$$0.4\ Na_2O : 10\ SiO_2 : 1.4\ Al_2O_3 : 16\ (TMA)_2O : 650\ H_2O.$$

With this composition, a slight yellow transparent solution is obtained when heated to the synthesis temperature of 95 °C.

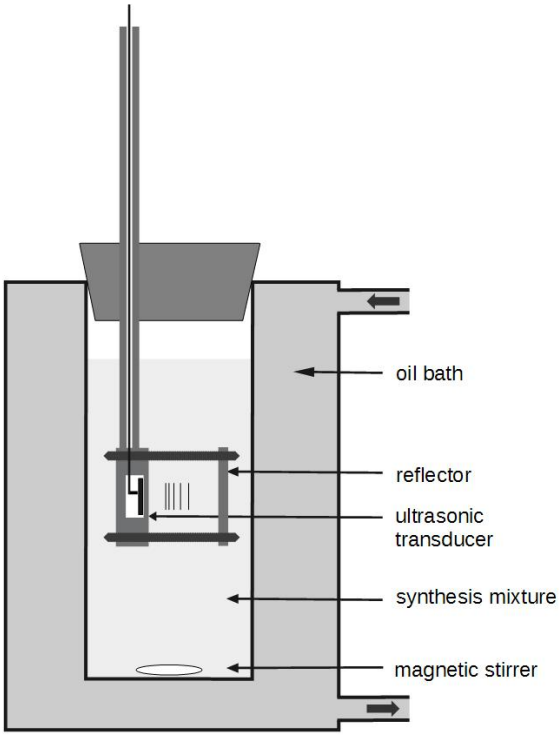

Figure 1: Experimantel setup: the ultrasonic measuring cell is placed inside the reaction mixture.

The prepared synthesis mixture was introduced into the autoclave with the ultrasonic measuring cell shown in Figure 1. The temperature was carried out using a thermostat-controlled circulating oil bath. A homogeneous convection of the synthesis mixture was maintained by magnetic stirring. The temperature of the colloidal solution was monitored with aid of a thermocouple inserted into the body of the ultrasonic probe.
The distance between the transducer with a main frequency of 2 MHz and the reflector was 30 mm. The ultrasonic attenuation travelling through the reaction fluid was measured in pulse-echo mode. Data acquisition was made by using PBP Optel software (Ver 4.1/2004).

X-ray powder diffraction pattern (XRD) for the phase identification and the estimation of the crystallinity were recorded on an X'Pert Pro diffractometer (Philips Analytical), using CuKα radiation. Peak areas were analyzed using the X'Pert Highscore software. To determine the relative crystallinity of the samples, the areas of four very intense XRD reflections hkl [200], [220], [622] and [642] at 2Theta ≅ 7.21° (12.28 Å) ; 10.20° (6.68 Å) ; 24.01° (3.70 Å) and 27.14° (3.28 Å) respectively, were summed. The sample with the highest value was set to 100 % and all the sample were normalized to this standard.

$$Crystallinity\,[\%] = \frac{\sum Area\ of\ the\ selected\ reflexes\ for\ each\ sample}{\sum Area\ of\ the\ selected\ reflexes\ for\ standard} \cdot 100$$

Scanning electron microscopy (ULTRA 55; Carl Zeiss AG) was used for qualitatively observing particle size and the particle size distribution. The elemental composition of the samples and the mother liquor were obtained by using inductively coupled plasma optical emission spectrometry (ICP-OES), performed on a Plasma 400 (Perkin Elmer). All solid samples were initially digested in a microwave for 45 minutes with a mixture of 2 ml of HNO_3, 2 ml of HCl and 8 ml of HF. Thereafter, the obtained aqueous sample was diluted with double deionized water in a 250 ml measuring flask and measured directly. The particle sizes were determined by dynamic light scattering (DLS) with a photon correlation spectrometer (Zetasizer 3000) from Malvern. The intensity data averaged from three consecutive measurements were used to estimate the particle size distribution.

Results

The progress of the ultrasonic attenuation and velocity during the colloidal synthesis of zeolite A at 95 °C is shown in Figure 2. The ultrasonic velocity shows no considerable change during the synthesis. The reason for this is that changes of the ion concentrations and of the density of the

mother liquor during crystallization are small. Thus, no measurable changes to the ultrasonic velocity are detected. It is important to mention that in the colloidal synthesis, the yield obtained in comparison to the synthesis from dense gels is very low (1.55 g of solid product per 100 g of synthesis solution).

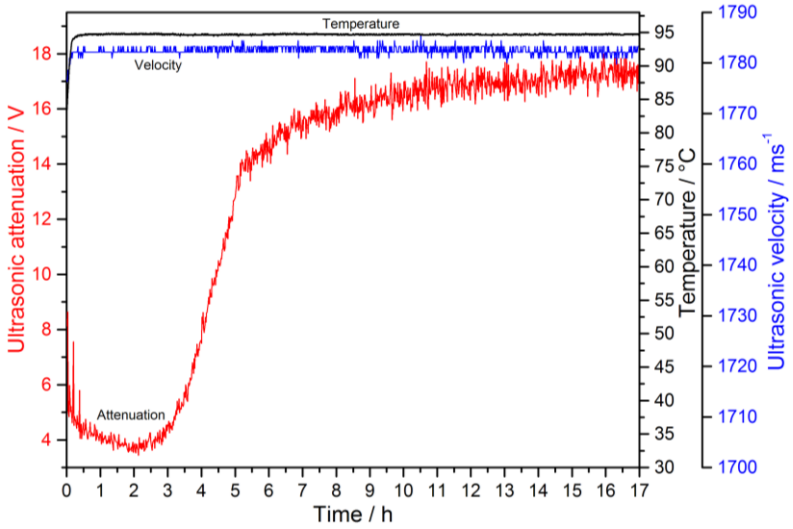

Figure 2: Progress of the ultrasonic attenuation (left, red) and velocity (right, blue) during the synthesis of colloidal zeolite A at a synthesis temperature of 95 ° C (black line). The overall molar composition of the starting synthesis gel was 0.4 Na_2O : 10 SiO_2 : 1.4 Al_2O_3 : 16 $(TMA)_2O$: 650 H_2O.

The progress of the ultrasonic attenuation can be divided into different stages. At the beginning of the synthesis, the US signals drops for approximately 2 hours. Due to the nearly direct contact with the preheated oil bath the temperature increases more rapidly compared to a classical steel autoclave. Thus, the targeted synthesis temperature is reached within a few minutes.

During this time, it was observed that the gel formed after mixing is dissolved in the mother liquor and forms a transparent, homogeneous synthesis solution. The dissolution of the amorphous gel particles leads to a decrease in the ultrasonic attenuation and it reaches a minimum value of about 3.6 volts after about 2 hours, the end of the first period – the homogeneity.

After 2 hours, the synthesis mixture begins to become cloudy andthe ultrasonic attenuation increases slowly. With increasing turbidity of the synthesis mixture, the ultrasonic attenuation increases further.

The sigmoidal curve of the ultrasonic attenuation here runs with different slopes. The steeper first phase ends after about 5.2 hours. In this time range, the value of the ultrasonic attenuation rises from 3.6 V to 13.9 V. In the second phase, the ultrasonic attenuation continuous with a lower slope

until it reaches the maximum after 15 hours. Here a rise in ultrasonic attenuation from 13.9 V to 17.2 V was observed. After about 15 hours, almost no further change in the ultrasonic attenuation is observed.

We have shown earlier that the crystallization of zeolite A from a colloidal solution can be precisely monitored with the aid of real time, in-situ ultrasonic attenuation measurement technique. A good correlation was observed between the ultrasonic attenuation and crystallinity of the solid products in synthesis from dense and opaque gels [28 - 31]. During the preliminary investigations, it was observed that only the quantity of zeolite changed over time in the synthesis of colloidal zeolites.

To verify this observation, samples were taken from the autoclave and the amount of zeolite was determined. The curve marked with blue squares in Figure 3 shows the amount of zeolite A formed from 100 g of sample over a period of 3.5 h to 7.5 h during ultrasonic measurement (sampling I). The curve marked with red cyrcles is a repetition of the experiment without ultrasonic measurement (sampling II). In this second repeat synthesis, samples were taken every hour to determine the particle size distribution by DLS (sampling II).

In Figure 3, the direct proportionality between the US attenuation and the amount of zeolite crystals is evident. More specifically, the ultrasonic attenuation signal correlates with the total volume of solid particles.

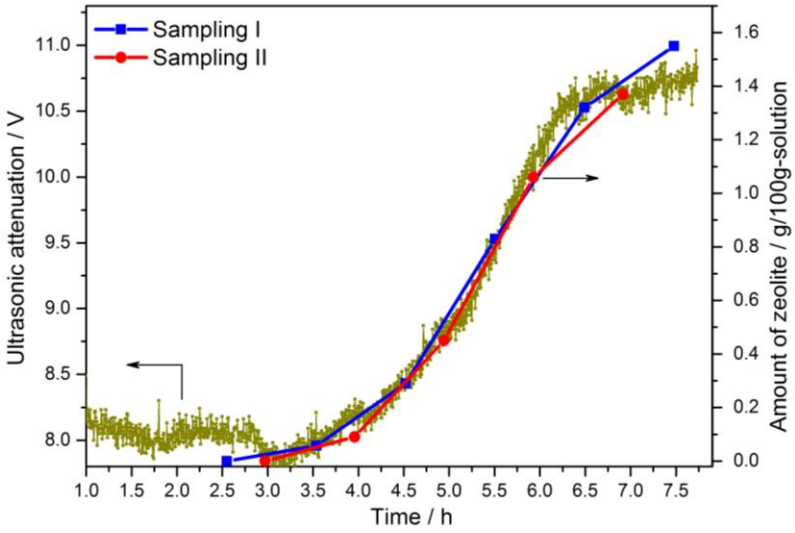

Figure 3: Progress of the in-situ measurement of the ultrasonic attenuation (yellow curve) compared with two series of ex situ sampling experiments (blue and red) for the synthesis of Zeolite A at 95 °C.

Acording to the scattering theory, the ultrasonic attenuation is directly proportional to the amount of zeolite crystals. The explanation is that the ultrasonic waves travel during the incubation period through the transparent solution without scattering. Thus, the ultrasonic attenuation values of the incubation period amounts to about 3.6 V. With the onset of the crystal formation, subsequent crystal growth and increasing size of the formed crystals, ultrasonic waves are scattered by solid particles according to their total amount. The larger the total volume, the more intense is the scattering.

The XRD pattern of zeolite A nanocrystals obtained in the present study matched very well with the simulated pattern given in the literature (Figure 4) [52]. The results of these ex-situ analyses are summerized in Table 1.

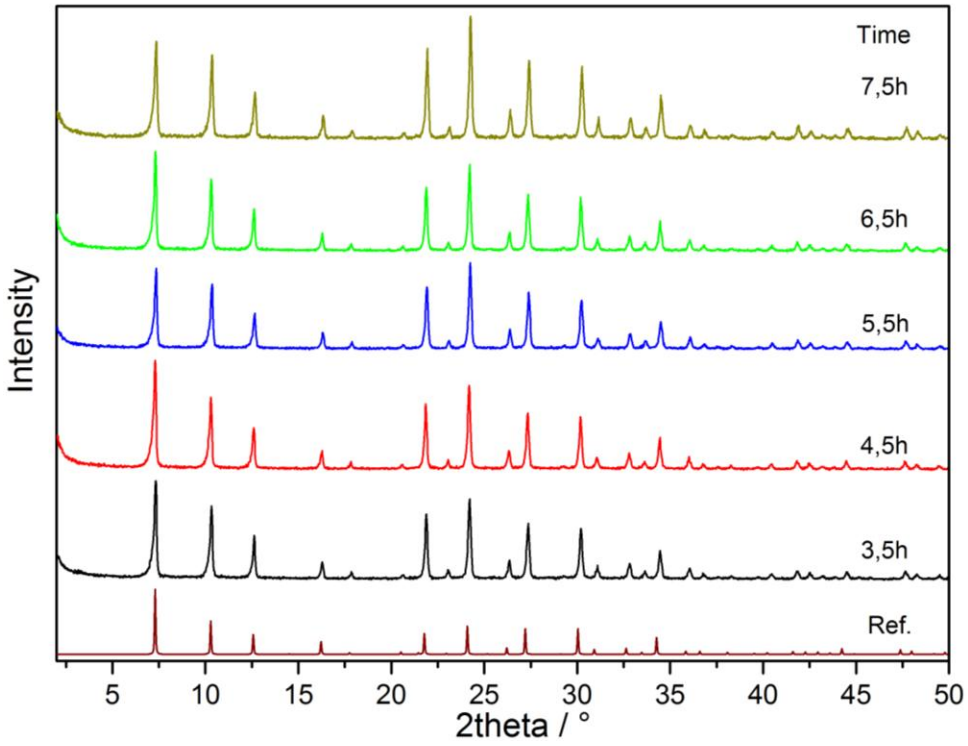

Figure 4: XRD patterns of samples (sampling series I) at different times; comparison with the simulated pattern (Ref.) of zeolite A.

Table 1: Results of the ex-situ analyses

Time / h	Yield / g [a]	Crystallinity / % [b]	Si concentration / mol·L^{-1} [c]	Al concentration / mol·L^{-1} [c]	Na concentration / mol·L^{-1} [c]
0	0.00	-	0.699	0.196	0.056
3.5	0.06	100	0.668	0.175	0.050
4	0.09	-	-	-	-
4.5	0.29	91	0.683	0.171	0.041
5	0.45	-	-	-	-
5.5	0.83	86	0.644	0.144	0.019
6	1.06	-	-	-	-
6.5	1.32	86	0.606	0.128	0.005
7	1.37	-	-	-	-
7.5	1.55	76	0.620	0.128	0.003

[a] Yield: Amount of zeolite g/100g solution (reaction mixture); [b] Crystallinity: the first sample at 3.5h was taken as reference; [c] Concentrations in liquid phase determined by ICP analyses

Time / h	1	2	3	4	5	6	7	8
Particle size / nm [d]	16	18	20	489	566	534	621	660

[d] Particle size was determined by DLS, the value of the maximum of the distribution hourly is given

For the determination of particle size and morphology of the crystals formed, samples were withdrawn from the synthesis mixture every hour during the crystal growth period between 4 and 7 h. The electron micrographs of the crystals (Figure 5) show a broad particle size distribution in all samples. While the crystals after the shorter times of about 4 h to 5 h are still round, the crystals at the extended times of about 6h and 7h show cubic shape with square edges.

According to these results, the following nucleation and crystal growth mechanism can be proposed. For the distribution of nuclei in the amorphous gel, there are two possiblities. Either the nucleation occurs on the external surface of the gel (classical heterogeneous nucleation) or inside the gel (homogeneous nucleation). The broad particle size distribution in SEM images (Figure 5)

indicates that the nuclei are located in the center of the gel and at the interface to the mother liquor.

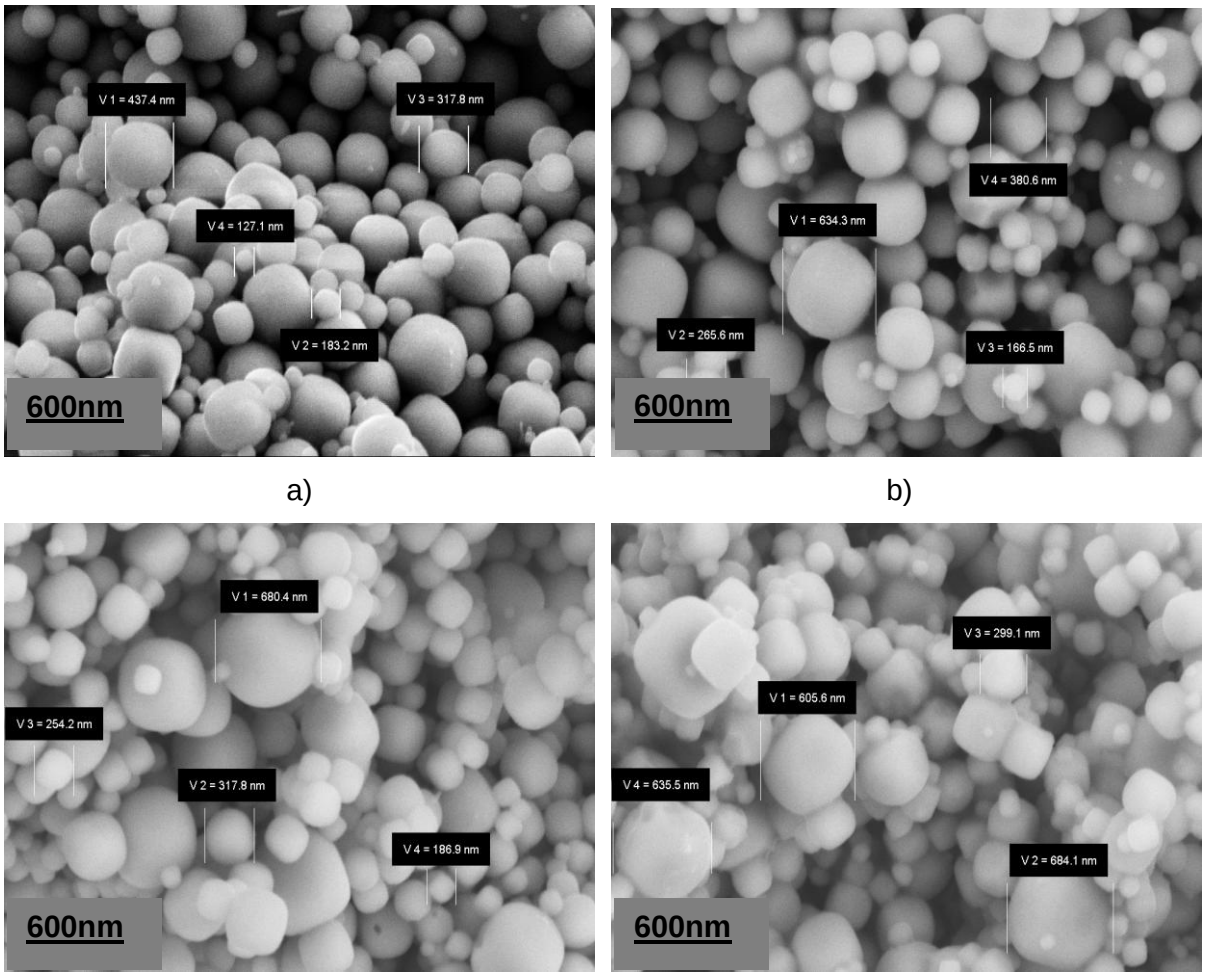

Figure 5: SEM images of the samples taken after 4 h (a), 5 h (b), 6 h (c) and 7 h (d), the particle size of selected specimen are highlighted to illustrate the distribution

After the formation of viable nuclei, the first phase of the crystal growth process begins. The growth of crystals from the nuclei is done by transport of the soluble species from the mother liquor to the nuclei. The crystals at the amorphous gel/mother liquor interface grow faster than the crystals in the center of the gel because they have direct contact with the mother liquor.

Li et al. [57] have observed during the microwave-assistant synthesis of LTA that after 25 min round-shaped particles with size of about 400 nm were formed. When the crystallization synthesis time was extended, well-shaped cubic LTA zeolite crystals with edge lengths of about 1 μm were obtained. The terrace feature of these crystals implies that between 25 and 35 min layer growth is the controlling mechanism during the crystallization. Similar changes can be assumed for our

systems if the crystallization time is prolonged and the crystals are growing even in this solution mediated hydrothermal synthesis.

Variation of the amount of water in the synthesis mixture

Water is quantitatively added to the synthesis mixture during hydrothermal zeolite synthesis. Its quantity influences the alkalinity of the mother liquor. The formation of saturated mother liquor by dissolving the gel and transporting the active species to the nuclei and growing zeolite crystals are fundamental steps in a synthesis, where the solvent is involved as a reservoir or transport medium.. Hydrolysis and condensation, where water is formed in the reaction, are fundamental reactions in the formation and transformation of the active species. The additional water would affect hydrolysis reactions and thus the formation of the active species. As a result, the incubation period should change with increase in the water content. However, since excess water is present here, this chemical effect can be excluded. Increasing the water content with a constant amount of other starting substances (especially NaOH and TMAOH) will lead to a decrease in alkalinity and dilution of the synthesis mixture.

To investigate the effect of the alkalinity and the dilution on the zeolite yield, particle size, and crystalization time, the water content was varied in the synthesis mixture (0.4 Na_2O : 10 SiO_2 : 1.4 Al_2O_3 : 16 $(TMA)_2O$: X H_2O (X = 650, 750, 850, 950), 1050). The temperature (95 °C) and all other synthesis parameters were kept constant.

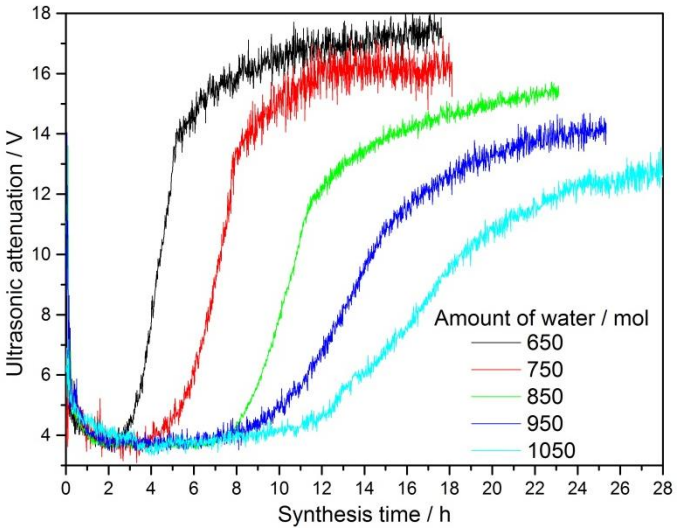

Figure 6: Progress of the ultrasonic attenuation as a function of the water content in the synthesis mixture: 10 SiO_2: 1.6 Al_2O_3: 0.4 Na_2O: 16 $(TMA)_2O$: X H_2O with X: 650 – 1050, (95°C)

The results of the ultrasonic attenuation measurement are displayed in Figure 6. The ultrasonic attenuation curves for the syntheses with higher amount of water (1050 mol and 950 mol) have a sigmoidal shape. An increase in water content leads to a prolongation of the incubation time and decrease of the crystallization rate. The shift of the crystallization onset (t_0) with increasing the amount of water is caused by the decrease in pH.

The ultrasonic attenuation curves have different heights. The reason for this is the dilution of the synthesis mixture (decrease in the solid concentration in the liquid phase). On the other hand, the yield decreases with increasing water content in the synthesis mixture. The yield of formed zeolite A amounts to 1.17 g (per 10 g Ludox HS-30) from the concentrated solution (650 mol H_2O), while ca. 0.89 g (per 10 g Ludox HS-30) zeolite A is formed from a more diluted solution (1050 mol H_2O). The increase in the amount of water means that the dissolved starting substances remain unreacted in the mother liquor (see Figure 7).

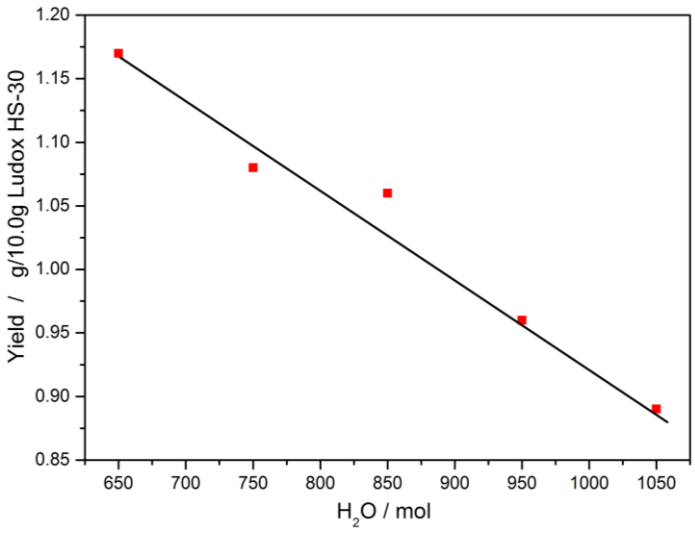

Figure 7: Change in product yield as a function of the amount of water in the synthesis mixture

Kinetic analysis of the ultrasonic attenuation data

For the kinetic analysis of the measured ultrasonic attenuation the above described models (Kerr, Ciric, Toufar, Avrami-Erofeyef, modified Avrami-Erofeyef and Gualtieri (equation 1, 3, 5, 6, 8 and 10, respectively) were used and the kinetic results were compared. First of all, the ultrasonic attenuation curves (Figure 6) were normalized so that the curves at the minimum have the value (0) and the value (1) at their maximum. The normalized ultrasonic attenuation curves are shown in Figure 8.

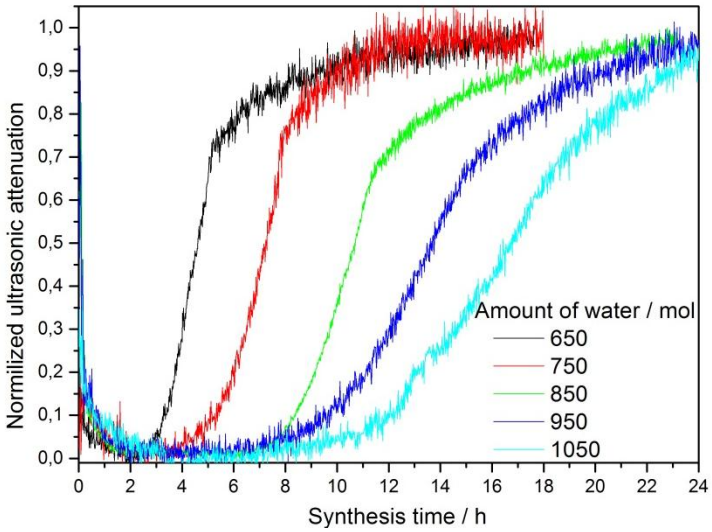

Figure 8: Normilized ultrasonic attenuation as a function of the water content in the synthesis mixture: $10SiO_2$: $1.6Al_2O_3$: $0.4Na_2O$: $16(TMA)_2O$: XH_2O, (T: 95°C), X . 650, 750, 850, 950 and 1050

Here, the time zero (t_0) (duration of incubation and the start of crystal growth) must be determined carefully. The size of t_0 influences the course of the linearized ultrasonic attenuation curve and a different slope is obtained. Thus, the value of t_0 affects the accuracy of the agreement of experimental and calculated data, as Schwieger et al. have shown for the kinetic investigation of the synthesis of magadiite [58].

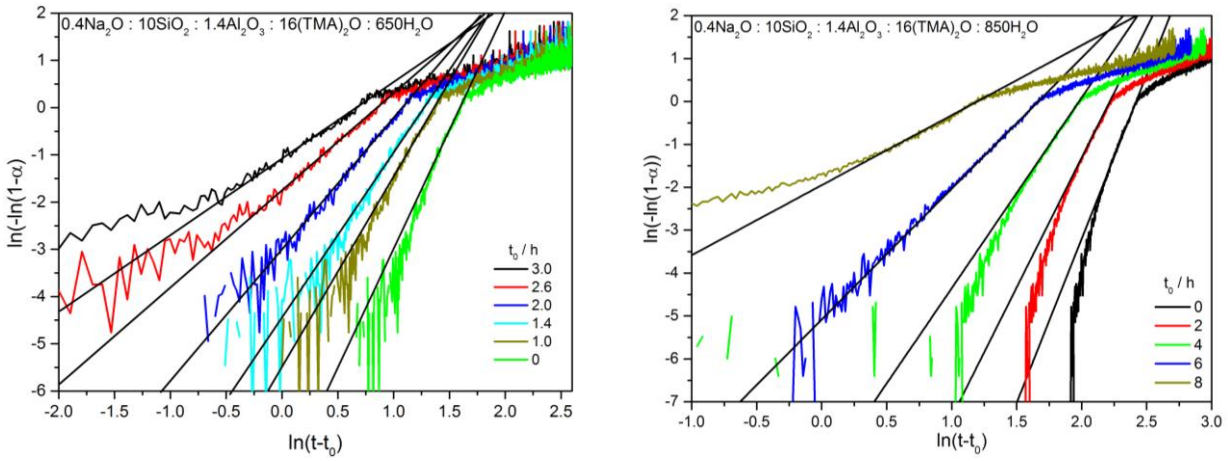

A) B)

Figure 9: Sharp-Hancock plot (Eq. 9) of the ultrasonic attenuation curves to show the influence of the time zero value (t_0) on the course of linearized curves for just two water contents (The molar composition of the synthesis gel was $0.4Na_2O : 10SiO_2 : 1.4Al_2O_3 : 16(TMA)_2O : X\ H_2O$; X : 650 (A) and X: 850 (B)).

Figure 9 shows as an axample the influence of the value of time zero (t_0) on the linearization of the ultrasonic attenuation curve. Here the values of t_0 were varied (A): from 0h to 3h and B): from 0h to 8h). One can clearly see that only for values of t_0: 2.0h in A) and for t_0: 6h in B) a good agreement between the experimental values and the fitted lines are obtained. At t_0 values smaller and larger than the correct t_0 value (t_0: 2.0h for A) and t_0: 6h for B)), the curves deviate either downwards or upwards from the fit line. For this value of (t_0) is the sum of of squares of the residuals, the difference between observed value and the fitted value, has a minimum.

In Table 2, the calculated kinetic parameters of the Sharp-Hancock plots (Figure 9) were listed. By varying the value of t_0, the value of the both two kinetic parameter (n and k) change. The Avrami exponent (n) increases linearly when t_0 becomes smaller. The reaction rate constant (k) shows an exponential dependence. As t_0 increases, the value of (k) increases. The determined kinetic parameters of the Table 2 were plotted in Figure 10.

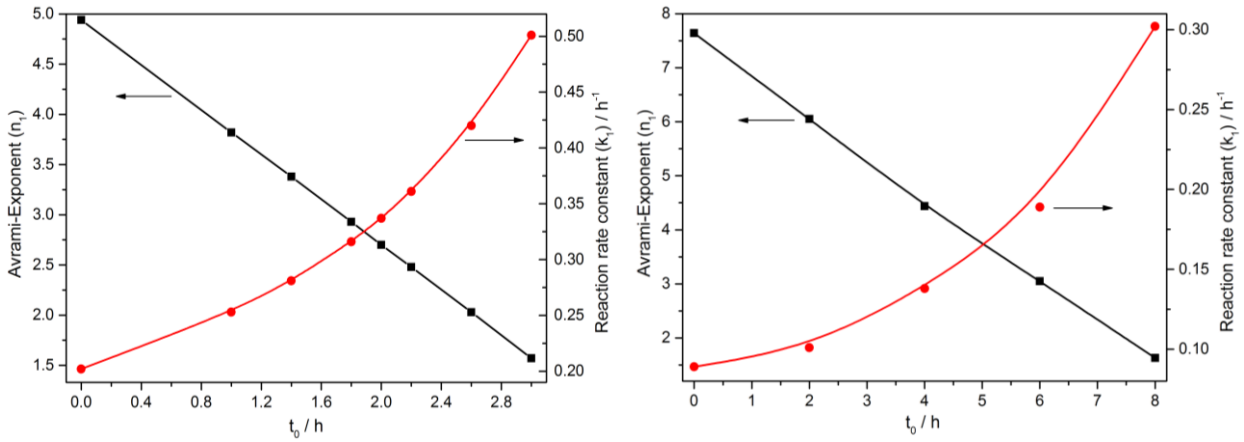

Figure 10: Representation of the results displayed in Table 2. The molar composition of the synthesis gel was 0.4 Na_2O : 10 SiO_2 : 1.4 Al_2O_3 : 16$(TMA)_2O$: X H_2O; A) X = 650 and B) X = 850.

Table 2: Impact of a choosen value of (t_0) on the determination of kinetic parameters (see also Figure 9 and 10).

0.4 Na_2O : 10 SiO_2 : 1.4 Al_2O_3 : 16 $(TMA)_2O$: 850 H_2O					
t_0 / h	Slope	Intercept	n	k / h^{-1}	$\sum_{\alpha:0.01}^{0.7} r_\alpha^2$
0	7.64	-18.48	7.64	0.089	234,59
2	6.05	-13.41	6.05	0.101	119,37
4	4.44	-8.79	4.44	0.138	46,52
6	**3.05**	**-5.08**	**3.05**	**0.189**	**4,1**
8	1.63	-1.95	1.63	0.302	118,02

0.4 Na_2O : 10 SiO_2 : 1.4 Al_2O_3 : 16 $(TMA)_2O$: 650 H_2O					
t_0 / h	**Slope**	**Intercept**	**n**	**k / h^{-1}**	$\sum_{\alpha:0.01}^{0.7} r_\alpha^2$
0	4.94	-7,91	4.94	0.202	21.87
1	3.82	-5,25	3.82	0.253	15.14
1.4	3.38	-4,29	3.38	0.281	10.99

1.8	2.93	-3,38	2.93	0.316	7.27
2.0	**2.70**	**-2.94**	**2.70**	**0.337**	**6.56**
2.2	2.48	-2,53	2.48	0.361	8.67
2.6	2.03	-1,76	2.03	0.420	108.97
3	1.57	-1,08	1.57	0.501	38.78

$\sum_{\alpha:0.01}^{0.7} r_\alpha^2$: The sum of squares of the residuals, the difference between observed and the fitted value

The values of (t_0) determined with the method described above are listed in the Table 3. The incubation period is prolonged also with increasing amount of water. In the syntheses with water contents higher than 850 mol, the incubation period amounts to a constant value of about 6 h. Probably the transport rate of the active species from the mother liquor to the seeds in the gel is the rate-limiting step in the nucleation phase.

Table 3: By applying the Sharp-Hancock plot (Eq. 9, Figure 9), the times of onset for the crystal growth (t_0) as a function of the amount of water in the synthesis gel composition is determined.

Amount of water / mol	**650**	**750**	**850**	**950**	**1050**
t_0 / h	2.0	3.6	6.0	6.0	6.0

The obtained values of induction times (t_0) were used for fitting of the experimentall curces with the models by Kerr, Ciric, Avrami and modified Avrami.

Figure 11 shows how the values of the crystallization rate constent were determined using the slope method of Culfaz and Sand [53].

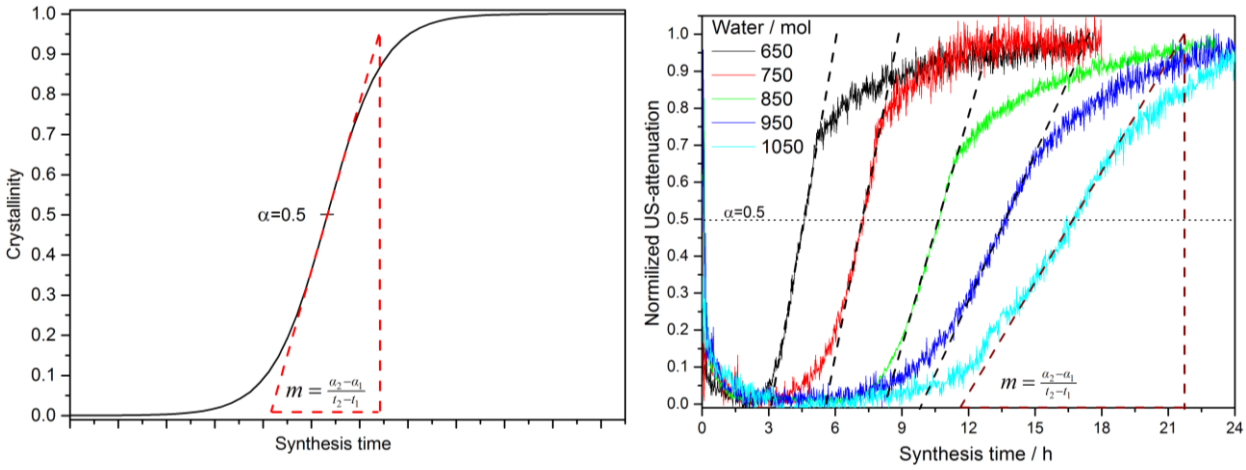

Figure 11: Determination of the crystallization rate employing the slope method by Culfaz and Sand [53].

Comparison of the crystallization models

In Figure 12 and 13, two ultrasonic attenuation curves of the synthesis with the highest (1050 mol of H_2O) and the smallest (650 mol of H_2O) amount of water in the synthesis mixture. Both curves were normalized and fitted with different kinetic models. These two curves are used for comparison, because they represent two extremes in fitting with the described kinetic models.The measured ultrasonic attenuation curves of the syntheses with higher water content (1050mol H_2O) in Figure 12 have a sigmoidal appearance. This experimentally determined crystallization process can be well described with four of six models. The two simple models of Kerr (exponential function) and Ciric (power function) can only describe the initial range of the crystal growth progress (Kerr α = 0.00 - 0.40; and Ciric α = 0.00 - 0.65).

As evident from Figure 13, the growth of crystals occurs with two different slopes. This means that the entire crystallization process consists of two growth steps. The first step of crystal growth occurs between α = 0.0 and α = 0.7. Subsequent second step lasts between α = 0.7 and α = 1.0. The existence of a second growth step confirms the observations of an equilateral extending homogeneous and heterogeneous nucleation mechanism, which will be explained below.

The models of Kerr (exponential function), Ciric (power function) and Toufar (sigmoidal function) can only be used to describe the initial range of the crystallization from α = 0.0 to α = 0.7. Although

the entire crystallization process can be described with the Gualtieri model, it cannot provide information about the two growth steps.

Two distinct regions were fitted separately with Avrami-Erofeyef and modified Avrami-Erofeyef model to yield pairs of rate constants and Avrami exponents for each region. The fitting curves for the first and second crystal growth steps are shown in Figure 13 in different colours. The fitting curves in the range from α = 0.0 to α = 0.7 are marked as Avrami 1 and modified Avrami 1 (red curves). In the remaining range from α = 0.7 to α = 1.0 they are named Avrami 2 or mod. Avrami 2 (blue curves).

Such a two-stage synthesis process has also been described by Millange et al. employing the Avrami-Erofeyev equation [59]. The authors have investigated the crystallization of $[Mg_3Al(OH)_8][(CO_3)_{0.5}].2H_2O$ with in-situ XRD. The Avrami-Erofeyev lines obtained from in-situ data consisted of two lines with different rate constants (k) and Avrami exponents (n). The determined kinetic parameters by the fitting of the ultrasonic attenuation curves with different models in the syntheses with different amounts of water from 650 to 1050 mol are collected in Table 4.

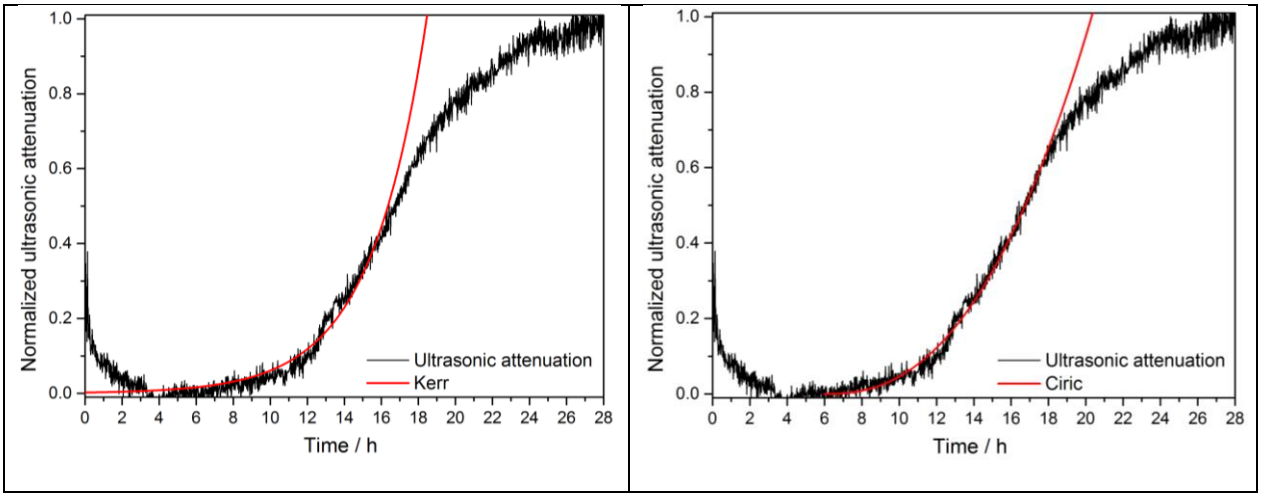

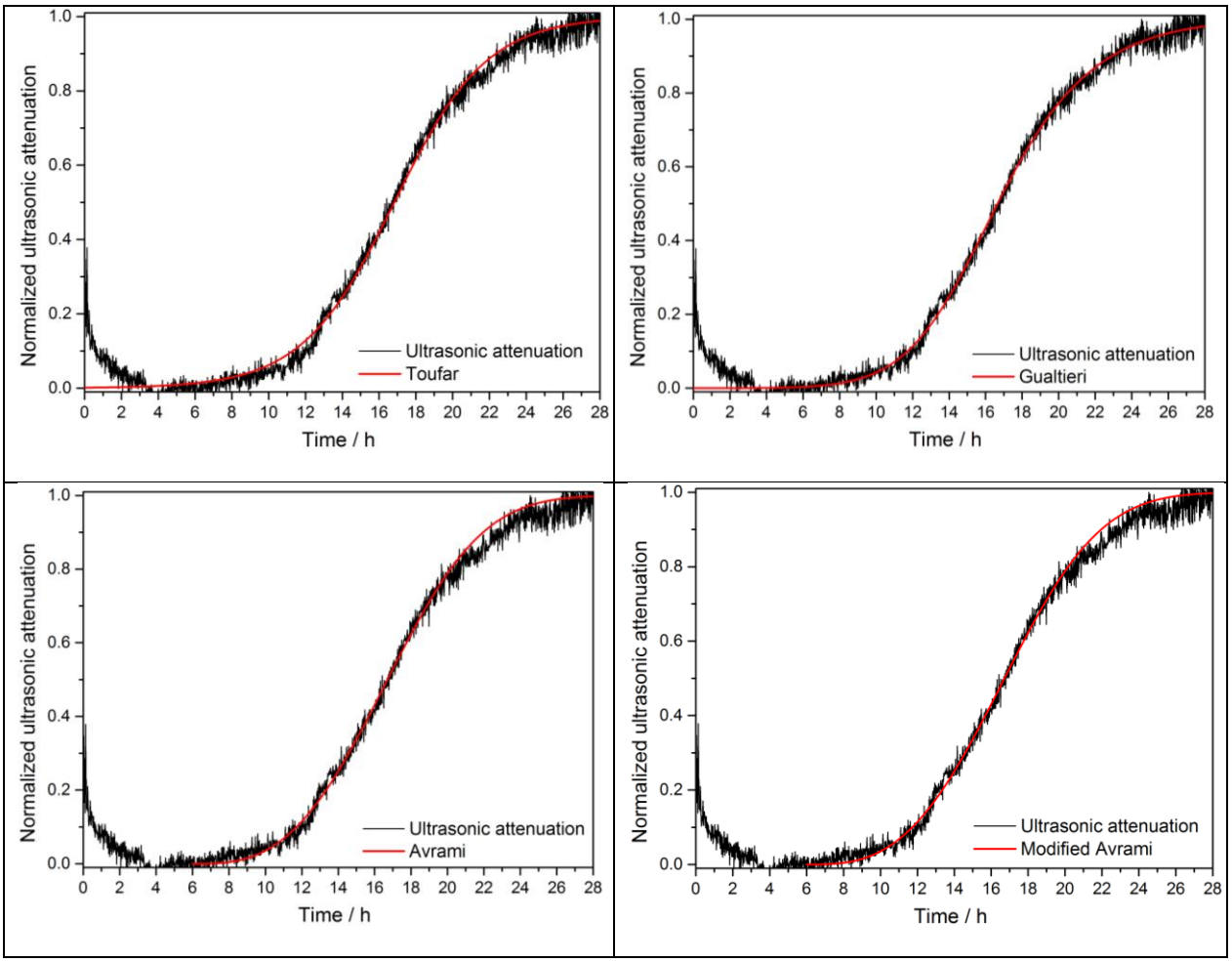

Figure 12: Comparison of fitting of the kinetic models to the experimentally determined crystallization process of colloidal zeolite A ($0.4Na_2O : 10SiO_2 : 1.4Al_2O_3 : 16(TMA)_2O : 1050H_2O$)

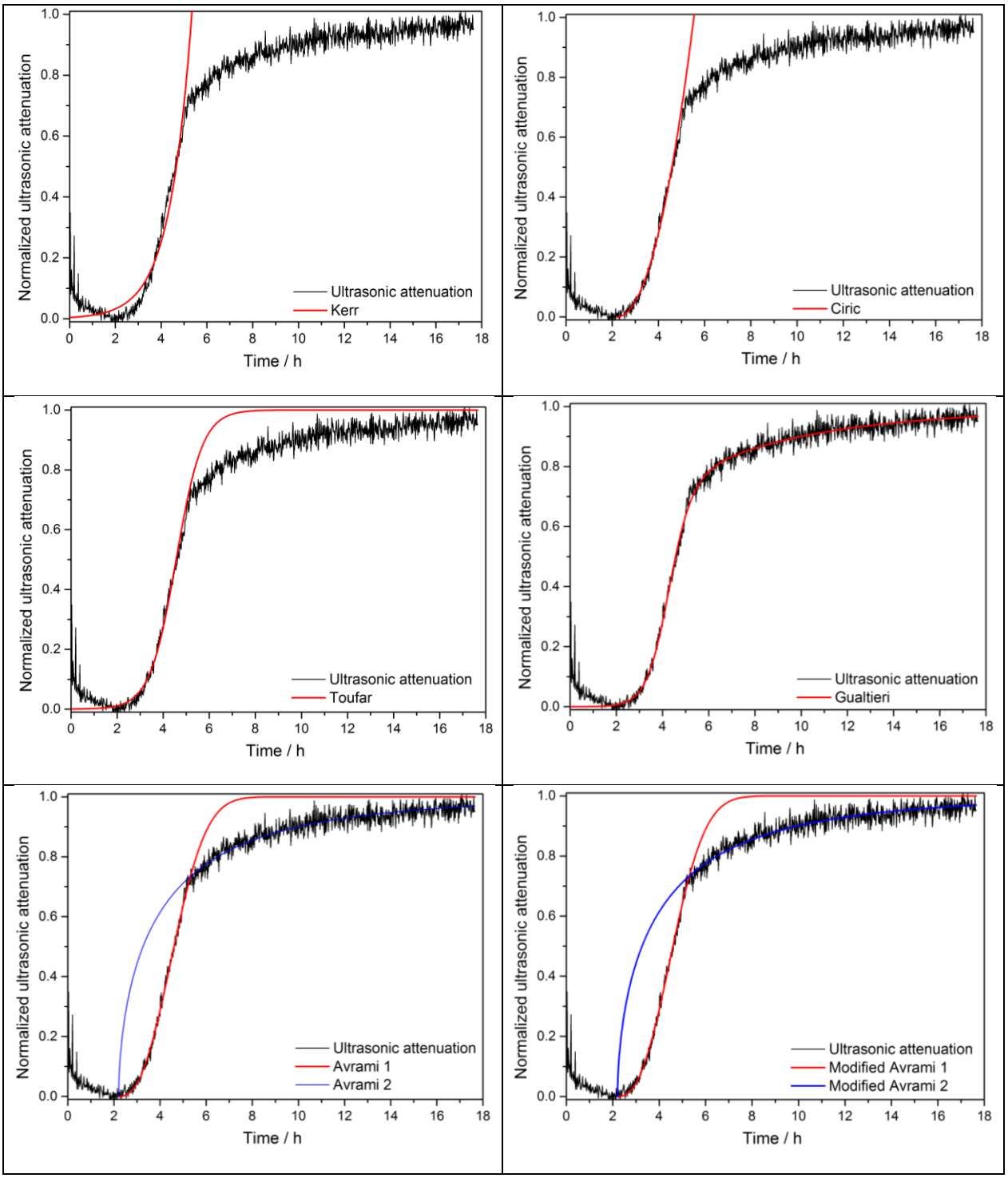

Figure 13: Comparison of the fits of the kinetic models to the experimentally determined crystallization process of colloidal zeolite A (0.4 Na_2O : 10 SiO_2 : 1.4 Al_2O_3 : 16 $(TMA)_2O$: 650 H_2O)

Table 4: Kinetic parameters determined by fitting of experimental curves with different modells.

Model	Range	Parameter	$0.4Na_2O : 10SiO_2 : 1.4Al_2O_3 : 16(TMA)_2O : X\ H_2O$				
			X=650	X=750	X=850	X=950	X=1050
Kerr	α =0 to α = 0.7	k	1.031	0.754	0.941	0.441	0.332
		α	0.039	0.031	0.010	0.020	0.016
Ciric	α = 0 to α = 0.7	k	0.083	0.030	0.012	0.006	0.002
		n	2.070	2.159	2.432	2.164	2.421
Toufar	α = 0 to α = 1.0	k	0.874	0.604	0.473	0.255	0.199
		t_l	4.563	7.208	10.647	13.758	16.828
Gualtieri	α = 0 to α = 1.0	a	4.200	6.860	9.860	12.490	14.820
		k_n	0.238	0.146	0.101	0.080	0.067
		b	0.490	0.760	0.880	1.780	2.430
		k_g	0.340	0.240	0.110	0.090	0.070
		N	0.690	1.030	1.250	1.370	2.210
Culfaz & Sand	α = 0 to α = 1.0	k	0.331	0.298	0.207	0.132	0.099
Avrami 1	α = 0 to α = 0.7	k_1	0.360	0.240	0.190	0.110	0.030
		n_1	2.540	2.770	2.800	2.820	3.040
Avrami 2	α = 0.7 to α = 1.0	k_2	0.490	0.310	0.210	0.120	0.090
		n_2	0.680	1.110	1.010	1.470	2.190
mod. Avrami 1	α = 0 to α = 0.7	k_1	0.079	0.021	0.010	0.004	0.0005
		n_1	2.493	2.678	2.762	2.581	3.079
mod. Avrami 2	α = 0.7 to α = 1.0	k_2	0.669	0.237	0.198	0.032	0.001
		n_2	0.603	1.193	1.015	1.610	2.748

As a simple exponential approach, the Kerr model only provides the rate constant. An increasing water amount in synthesis mixtures from 650 mol to 1050 mol results in a decreased crystal growth rate (see Table 4). The amount of water determines the concentration of the gel if the other parameters in synthesis composition are kept constant. The transport of the nutrients to the nucleation and crystal growth sites is hampered by dilution. Another important effect is the decrease in alkalinity. At a lower alkalinity, the dissolution rate of the amourphous gel is slow, thus the nutrient concentration may not be maintained.

Compared to Kerr [36], Ciric [37] provides an additional kinetic constant, the exponent (n). According to the model, the value of the exponent (n) gives information on the nucleation and crystal growth mechanism. If n = 3, the nucleation is heterogeneous, if n = 4 nucleation is homogeneous and in the case of n > 4, the nucleation is autocatalytic [60]. The resulting values of exponent (n) in this work for the 'Ciric' approach range between 2.2 and 2.5. Accordingly, nucleation is likely to be heterogeneous.

Toufar's [33] model can well reproduce a sigmoidal crystallization curve as shown in Figure 12. The model fails if the crystallization does not take place in a simple sigmoidal form (see Figure 13). The Toufar model delivers only the crystallization rate constant (k) in its valid crystallization range. The crystallization parameter t_0 is replaced with t_l, the sum of the time interval of the nucleation and the half-life of the crystal growth.

The values of nucleation and crystal growth rate (k_n and k_g respectively), the coefficient of distribution of the probality of nucleation (b), and the coefficient indicating the maximum rate of nucleation (a), extracted with the Gualtieri model are listet in Table 4. All values of k_n are smaller than k_g, indicates that the nucleation seems to be the rate-limiting process. Furthermore since $b \leq 15$, it can be interpreted that the nucleation proceeds in a heterogeneous fashion.Crystallization rate constants calculated with slope method of Culfaz and Sand are inserted in the table as a comparison. Compared to the other models, Avrami-Erofeyef approach can describe crystallization processes in a purely sigmoidal form as well as processes consisting of two steps. It is shown in Figure 13 that the Avrami Erofeyev plots consist of two curves. The more concentrated (less water) the synthesis mixture, the pore pronounced is the observed kink. The course with the largest amount of water (1050 mol) has a small kink. The Sharp-Hancook plot of the Avrami model in Figure 9 displays this in a better way. Because the Avrami Erofeyev plots consist of two parts, for both steps of crystal growth the Avrami exponent (n) (from slopes) and the rate constants (k) (from intersept on Y- Axis) can be calculated. The Avrami exponent for the first step of crystal growth

increases with dilution (viz. increasing of water amount). The value n_1 is for concentrated solution (650 mol water) amonuts to 2.5, while the value for diluted solution (1050 mol water) is about 3.0. The value of the Avrami exponent gives information on the dimension of the crystal growth [38,39]. A value of n = 1 shows surface crystallization (one-dimensional growth), whereas a value of n = 3 indicates a three-dimensional growth.

Interestingly, the Avrami exponent (n_2) for the second step of crystal growth is different. The lowest value of n_2 = 0.7 for is calculated for the smallest amount of water (650 mol of water). The larger the water amount, the higher is the Avrami exponent (e.g. n_2: 2.2 for 1050 mol). The Avrami exponent (n_2) has a value below 1, if the molar water content is lower then 850 mol. This is an indication for a one-dimensional crystal growth. In this second stage, well-formed cubic crystals with sharp edges (see Figure 5: more round particles in 5a and 5b in comperison to cubic particles in 5c and 5d) are formed. In consequence, the crystallization is controlled in the second stage by a layer-growth mechanism where the nutrients are transported through the liquid phase onto the crystal surfaces. The nutrients for this second step will be provided by dissolving the remaining gel or less stable zeolite crystals available in the reaction mixture (Ostwald ripening). This crystallization step, where a layer growth mechanism controls the zeolite formation, has been studied with Atomic Force Microscopy (AFM) and described in detail by Agger et al. [26].

From the ultrasonic curve in Figure 8 it can be seen that the second growth step for the synthesis with a water content of 750 begin at approx. 7 h. Accordingly, after this time the formed crystals should change their shape from round to cubic. In order to observe this, the obtained crystals were analayzed using SEM. The SEM images in Figure 14 show that crystals change their morphology from round to cubic with increasing crystallization time. After 30 h, almost all crystals have a cube-like shape.

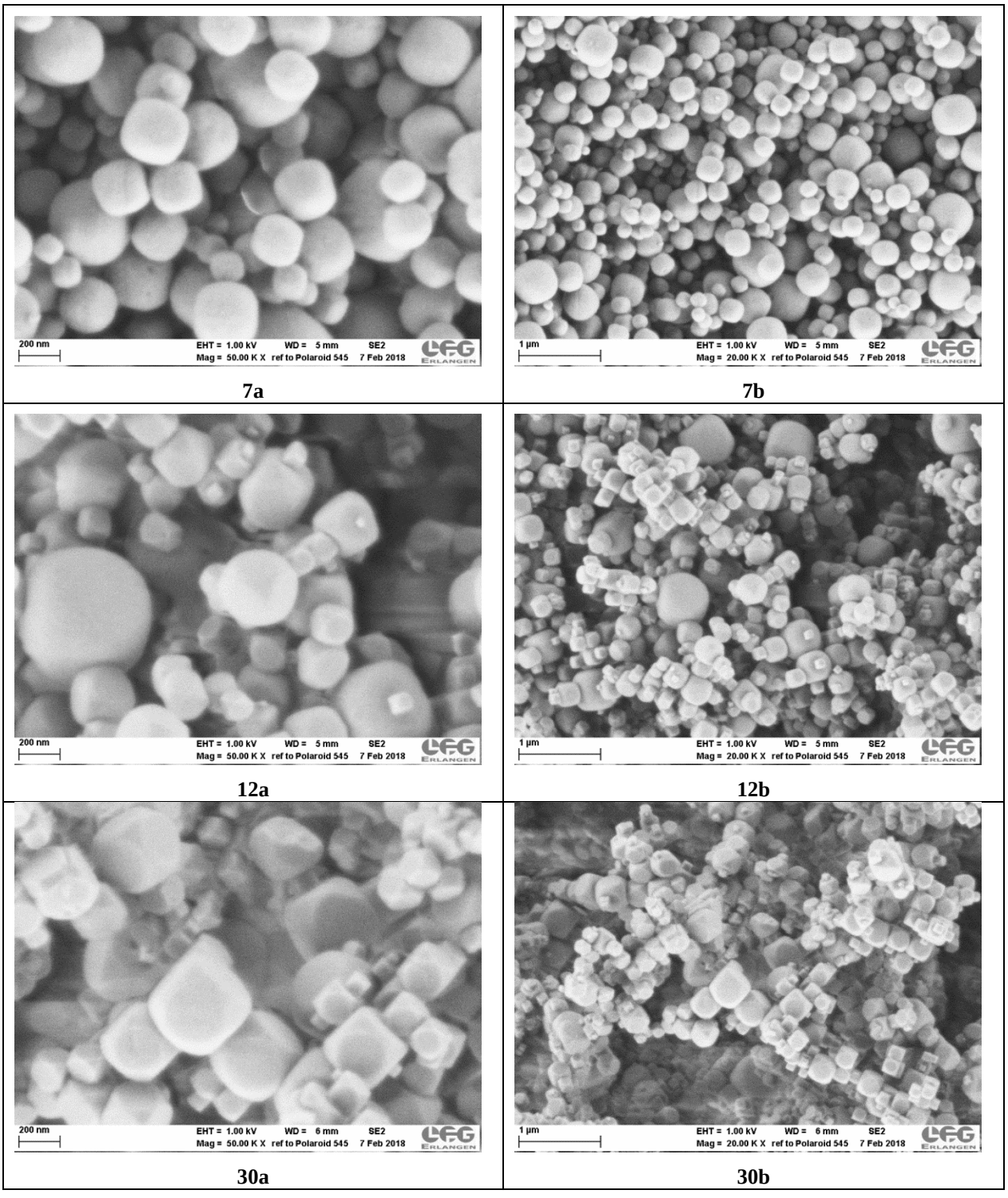

Figure 14: SEM images oft he samples taken after 7h (7a, 7b), 12h (12a, 12b) and 30h (30a, 30b) during the synthesis of the colloidal zeolite A with a molar water amount of 750.

Conclusions

In this work, the crystallization of zeolite A from a colloidal solution with the composition of 0.4 Na_2O : 10 SiO_2 : 1.4 Al_2O_3 : 16 $(TMA)_2O$: X H_2O was investigated by means of ex situ methods and a simple in situ US measurement. The amount of water (X) in synthesis mixture was varied from 650, 750, 850, 950 mol to 1050mol to study its impact on the crystallization kinetics. The crystallization process was followed directly by in situ ultrasonic attenuation measurements. Different mathematical models were used to extract kinetic data and the results were compared with each other to jugde the applicability of the different models.

It has been shown that the models of Ciric, Kerr and Toufar can only describe the initial range of the crystallization process from α =0.0 to about α = 0.7. They provide the reaction rate constant only for this range. In contrast, the model of Gualtieri describes the whole process, but cannot recognize the different crystallization steps, as shown here for the crystallization of zeolite A from colloidal suolutions. However, with the constants (k_n, a and b), information can be obtained to describe the nucleation process.
The best result was obtianed when the model of Avrami-Erofeyef was employed. As shown above the value of the Avrami exponent contains information about the mechanism of the crystallization. This model provides mathematical evidence that the crystallisation process of colloidal zeolite A consists of two steps where as a result crystals with different morpholgies are formed.

AUTHOR INFORMATION

Corresponding Authors

Wilhelm Schwieger – Institute of Chemical Reaction Engineering (CRT), Friedrich-Alexander-Universität Erlangen-Nürnberg (FAU), Egerlandstraße 3, 91058 Erlangen, Germany; orcid.org/0000-0003-4791-2667

Martin Hartmann - Erlangen Center for Interface Research and Catalysis (ECRC), Catalysis and Sustainable Processes, Friedrich-Alexander-Universität Erlangen-Nürnberg (FAU), Egerlandstraße 3, 91058 Erlangen, Germany; orcid.org/0000- 0003-1156-6264

Author

Hasan Baser - Institute of Chemical Reaction Engineering (CRT), Friedrich-Alexander-Universität Erlangen-Nürnberg (FAU), Egerlandstraße 3, 91058 Erlangen, Germany

Author Contributions

The manuscript was written through contributions of all authors. All authors have given approval to the final version of the manuscript.

Funding Sources

Any funds used to support the research of the manuscript should be placed here (per journal style).

Notes

The authors declare no competing financial interest.

ACKNOWLEDGMENT

W.S and H.B. gratefully acknowledge funding by the German Research Council (DFG), which supports the Cluster Excellence “Engineering of Advanced Materials” at the University of Erlangen-Nürnberg.
M.H. gratefully acknowledges financial support by the Deutsche Forschungsgemeinschaft (DFG, German Research Foundation), project-ID: Ha2527/16-1, project number: 445323933

References

[1] W. Bensch, N. Pienack, In-situ-Verfolgung der Bildung kristalliner Feststoffe. Angewandte Chem. 2011, 123, 2062 – 2083.

[2] R.Grizzetti, G, Artioli, Kinetics of nucleation and growth of zeolite LTA from clear solution by in situ and ex situ XRPD. *Microporous Mesoporous Mater*., 2002, 54,105–112.

[3] L. Gora, K. Streletzky, R. W. Thompson, G. D. J. Phillies, Study of the crystallization of zeolite NaA by quasi-elastic light-scattering spectroscopy and electron microscopy. *Zeolites,* 1997, 18, 119-131.

[4] M. E. Davis, R. F. Lobo, *Zeolite and molecular sieve synthesis.* Chem. Mater., 1992, 4 , 756-768

[5] M. Sánchez, J. Pérez-Pariente, C. Márquez-Álvarez, In situ ATR-FTIR for monitoring the kinetics of mesoporous molecular sieves synthesis. In *Stud. Surf. Sci. Catal.*, 2005; 158, 113-120.

[6] F. Fan, Z. Feng, C. Li, UV Raman spectroscopic study on the synthesis mechanism and assembly of molecular sieves. *Chem. Soc. Rev.,* 2010, 39 (12), 4794-4801.

[7] J. D. Epping, B. F. Chmelka, Nucleation and growth of zeolites and inorganic mesoporous solids: Molecular insights from magnetic resonance spectroscopy. *Current opinion in colloid & interface science,* 2006, *11* (2-3), 81-117.

[8] I. I. Ivanova, Y. G. Kolyagin, I. A. Kasyanov, A. V. Yakimov, T. O Bok, D. N. Zarubin, Time-Resolved In Situ MAS NMR Monitoring of the Nucleation and Growth of Zeolite BEA Catalysts under Hydrothermal Conditions. *Angew. Chem. Int. Ed.,* 2017, *56* (48), 15344-15347.

[9] M. G. O'Brien, A. M. Beale, B. M. Weckhuysen, B. M., The role of synchrotron radiation in examining the self-assembly of crystalline nanoporous framework materials: from zeolites and aluminophosphates to metal organic hybrids. *Chem. Soc. Rev.,* 2010, *39* (12), 4767-4782.

[10] S. Mintova, N. H. Olson, V. Valtchev, T. Bein, Mechanism of zeolite A nanocrystal growth from colloids at room temperature. *Science,* 1999, 283, 958 -960.

[11] S. L. Anderson, A. Gładysiak, P.G. Boyd, C. P. Ireland, P. Miéville, D. Tiana, B. Vlaisavljevich, P. Schouwink, W. Van Beek, K.J. Gagnon, K. J., Formation pathways of metal–organic frameworks proceeding through partial dissolution of the metastable phase. *CrystEngComm*., 2017, 19 (25), 3407-3413

[12] P. Norby, Hydrothermal conversion of zeolites: an in situ synchrotron X-ray powder diffraction study. *JACS,* 1997, *119* (22), 5215-5221.

[13] P. Norby, In-situ XRD as a tool to understanding zeolite crystallization. *Current opinion in colloid & interface science,* 2006, *11* (2-3), 118-125.

[14] G. Sankar, W. Bras, W., Insights into the formation of microporous materials by in situ X-ray scattering techniques. *Catal. Today,* 2009, *145* (3-4), 195-203.

[15] M. Kumar, M.K. Choudhary, J. D. Rimer, Transient modes of zeolite surface growth from 3D gel-like islands to 2D single layers. *Nat. Commun.,* 2018, *9* (1), 1-9.

[16] M. Tatlıer, M. Elnekave, Electrochemical monitoring of zeolite synthesis. *Mater. Chem. Phys.,* 2005, *91* (1), 99-103.

[17] G. Cao, M.J. Shah, In situ monitoring of zeolite crystallization by electrical conductivity measurement: New insight into zeolite crystallization mechanism. *Micropor Mesopor Mater.,* 2007, *101*, 19-23.

[18] G. Brabants, S. Lieben, L. Breynaert, E.. Reichel, F. Taulelle, F.; Martens, J.; Jakoby, B.; Kirschhock, C., Monitoring early zeolite formation via in situ electrochemical impedance spectroscopy. *Chem. Commun.,* 2016, *52* (31), 5478-5481.

[19] S.A. Pelster, R. Kalamajka, W. Schrader, F. Schüth, Monitoring the nucleation of zeolites by mass spectrometry. *Angew. Chem.,* 2007, *119* (13), 2349-2352.

[20] I. H. Lim, W. Schrader, F. Schüth, The formation of zeolites from solution–Analysis by mass spectrometry. *Micropor Mesopor Mater.,* 2013, *166*, 20-36.

[21] L. R. Follens, E. K. Reichel, C. Riesch, J. Vermant, J. A. Martens, C.E. Kirschhock, B. Jakoby, Viscosity sensing in heated alkaline zeolite synthesis media. *PCCP,* 2009, *11* (16), 2854-2857.

[22] S. Yang, SA. Navrotsky, B.L. Phillips, In situ calorimetric, structural, and compositional study of zeolite synthesis in the system 5.15 Na2O− 1.00 Al2O3− 3.28 SiO2− 165H2O. *The Journal of Physical Chemistry B,* 2000, *104* (25), 6071-6080

[23] S. Mintova, J.P. Gilson, V. Valtchev, Advances in nanosized zeolites. *Nanoscale*, 2013, *5*, 6693-6703

[24] M. Smaihi, O. Barida, V. Valtchev, Investigation of the crystallization stages of LTA-type zeolite by complementary characterization techniques*. Eur. J. Inorg. Chem.,* 2003, 2003, 4370-4377

[25] P. Cubillas, M. W. Anderson, Synthesis Mechanism: Crystal Growth and Nucleation, S.: 10- 55 (Published in: J. Cejka, A. Corma, S. Zones, Zeolites and Catalysis, Synthesis, Reactions and Applications, Weinheim, 2010, Vol. 1.)

[26] J. R. Agger, N. Pervaiz, A. K. Cheetham, M. W. Anderson, Crystallization in zeolite A studied by atomic force microscopy. *J. Am. Chem. Soc.,* 1998, 120, 10754-10759.

[27] M. Schmachtl, T. J. Kim, W. Grill, R. Herrmann, O. Scharf, W. Schwieger, R. Schertlen, C. Stenzel, Ultrasonic monitoring of zeolite synthesis in real time. *Ultrasonics,2000,* 38, 809.

[28] R. Herrmann, W. Grill, T. J. Kim, O. Scharf, R. Schertlen, M. Schmachtl, W. Schwieger, C. Stenzel, H. Toufar, Y. Venot, In-situ diagnostic of zeolite crystal growth by real time ultrasound monitoring. *Stud. Surf. Sci. Catal.,* 2001, 135, 195.

[29] R. Herrmann, W. Schwieger, O. Scharf, C. Stenzel, H. Toufar, M. Schmachtl, W. Grill, In situ diagnostics of zeolite crystallization by ultrasonic monitoring. *Microporous and Mesoporous Materials*, 2005, 80*,* 1-9.

[30] N. M. Musyoka, L. F. Petrik, E. Hums, H. Baser, W. Schwieger, In situ ultrasonic monitoring of zeolite A crystallization from coal fly ash. Catalysis Today, 2012, 190, 38–46.

[31] E. Hums, N. M. Musyoka, H. Baser, A. Inayat, W. Schwieger, In-situ ultrasound study of the kinetics of formation of zeolites Na–A and Na–X from coal fly ash. Res. Chem. Intermed, 2015, 41, 4311–4326.

[32] L. Tosheva, V. P. Valtchev, Nanozeolites: synthesis, crystallization mechanism, and applications. *Chem. Mater.,* 2005, 17, 2494-2513.

[33] H. Toufar, K.P: Wendlandt, H.G. Karge, A simple model for the kinetic evaluation of zeolite crystallization processes. *Journal of the Chemical Society, Faraday Transactions*, 1995, *91*(3), 549-554.

[34] B. Mihailova S. Mintova, K. Karaghiosoff, T. Metzger, T. Bein, Non-destructive identification of colloidal molecular sieves stabilized in water. *J. Phys. Chem. B*, 109, 2005, 17060-17065.

[35] R. A. Rakoczy Y. Traa, Nanocrystalline zeolite A: synthesis, ion exchange and dealumination. *Microporous and Mesoporous Materials,* 60, 2003, 69-78.

[35] L. Tosheva, V. P. Valtchev, Nanozeolites: synthesis, crystallization mechanism, and applications. Chem. Mater., 17, 2005, 2494–2513.

[36] G. T. Kerr, Chemistry of Crystalline Aluminosilicates, I. Factors Affecting the Formation of Zeolite A. *J. Phys. Chem.,* 1966, 70(4), 1047-1050.

[37] J. Ciric, Kinetics of zeolite A crystallization. *Journal of Colloid and Interface Science,* 1968, 28, 315-324.

[38] M. Avrami, Kinetics of Phase Change. I General Theory, *J. Chem. Phys.*, 1939, 7, 1103-1112.

[39] M. Avrami, Kinetics of phase change. II transformation-time relations for random distribution of nuclei. *J. Chem. Phys*., 1940, 8, 212-224.

[40] B.V. Erofeev, Generalized equation of chemical kinetics and its application to reactions with the participation of solid materials. *Dokl. Akad. Nauk SSSR. Nov. Ser.*, 1950, *73*(3), 515-528.

[41] V.K. Ueberreiter, K. Steiner, Kristallisationskinetik von polymeren 2. Mitteilung: Untersuchungen der Anwendbarkeit der AVRAMI-Gleichung auf den Kristallisationsverlauf von Polyäthylensuccinat. *Die Makromolekulare Chemie,* 1966, 91, 175-194.

[42] W. Schwieger, W. Heyer, K. H. Bergk, Die hydrothermale Kristallisation des Magadiits. 1. Die Kristallisationskinetik-Möglichkeiten ihrer Beschreibbarkeit. *Z. anorg. allg. Chem.*, 1988, 569, 191-200.

[43] J. D. Hancock, J. H. Sharp, Method of comparing solid-state kinetic data and its application to the decomposition of kaolinite, brucite, and BaCO3. J. Am. Ceram. Soc., 1972, 55, 74-77.

[44] D. Braga, M.R. Chierotti, N. Garino, R. Gobetto, F. Grepioni, M. Polito, A. Viale, Cis− Trans Isomerization in Crystalline [(η5-C5H5) Fe (μ-CO)(CO)] 2. *Organometallics,* 2007, 26, 2266-2271.

[45] C. Kosanovic, B. Subotic, E. Kranjc, Kinetic analysis of isothermal crystallization of low-carnegieite from precipitated amorphous aluminosilicate precursor. *Microporous and Mesoporous Materials,* 2004, 71, 27–32.

[46] F. Millange, R. El Osta, M. E. Medina, R. Walton, A time-resolved diffraction study of a window of stability in the synthesis of a copper carboxylate metal–organic framework. *CrystEngComm.***,** 2011, 13, 103–108.

[47] R. I. Walton, F. Millange, D. O'Hare, A. T. Davies, G. Sankar, C. R. A. Catlow, An in situ energy-dispersive X-ray diffraction study of the hydrothermal crystallization of zeolite A. 1. Influence of reaction conditions and transformation into sodalite. *J. Phys. Chem. B,* 2001, 105, 83-90.

[48] R. Walton, D. O'Hare, An in situ energy-dispersive X-ray diffraction study of the hydrothermal crystallization of zeolite A. 2. Effect of deuteration on crystallization kinetics. *J. Phys. Chem. B* 2001, 105, 91 – 96.

[49] C. Hübert, P. Starke, E. Rönsch, O. Rademacher, I. Fleddermann, Untersuchungen zum Alkalischen Abbau von Kieselgelen mittels Leitfähigkeitsmessungen*. Z. anorg. allg. Chem.*, 1985, 522, 217-225.

[50] L. Engelke, M. Schaefer, F. Porsch, W. Bensch, In-situ Energy-Dispersive X-ray Diffraction Studies of Crystal Growth and Compound Conversion under Solvothermal Conditions. Eur. J. Inorg. Chem. 2003, 506-513.

[51] L. Mandelkern, Growth and Perfection of Crystals, Wiley-Verlag, New York 1958; Crystallization of Polymers, McGraw-Hill, New York 1964, p. 229; zitiert in: V.K. Ueberreiter, K. Steiner, Kristallisationskinetik von polymeren 2. Mitteilung: Untersuchungen der anwendbarkeit der AVRAMI-Gleichung auf den Kristallisationsverlauf von Polyäthylensuccinat. Die Makromolekulare Chemie 91, 1966, 175-194.

[52] A. F. Gualtieri, Synthesis of sodium zeolites from a natural halloysite, *Phys. Chem. Miner.,* 2001, 28, 719 – 728.

[53] A. Culfaz, L.B. Sand, Mechanism of nucleation and crystallization of zeolites from gels, Adv. Chem. Ser. 121(1973) 140-151.

[54] H. Baser, T. Selvam, J. Ofili, R. Herrmann, W. Schwieger, In-situ ultrasonic methods for monitoring the hydrothermal synthesis of LTA-type zeolite from colloidal solutions. *Studies in surface science and catalysis* 2007; 170, 480-486.

[55] F. Babick, F. Hinze, M. Stintz, S. Ripperger: Ultrasonic spectrometry for particle size analysis in dense submicron suspensions. *Particle & Particle Systems Characterization: Measurement and Description of Particle Properties and Behavior in Powders and Other Disperse Systems*, 1998, 15, 230-236

[56] J. J. Pluth, J. V. Smith, Accurate redetermination of crystal structure of dehydrated zeolite A. Absence of near zero coordination of sodium. Refinement of silicon, aluminum-ordered superstructure. *J. Am. Chem. Soc.,* 1980, 102, 4704.

[57] Y. Li, J. Liu, W.Yang, Formation mechanism of microwave synthesized LTA zeolite membranes. *Journal of Membrane Science*, 2006, 281, 646–657.

[58] W. Schwieger, P. Grabner, H. Utschick, U. Brenn, W. Kunze, Thermoanalytische Untersuchungen an aluminiumfreien Schichtsilikaten. *Journal of Thermal Analysis and Calorimetry*, 1996, *47*, 407-418

[59] F. Millange, R. I. Walton, D. O'Hare, Time-resolved in situ X-ray diffraction study of the liquid-phase reconstruction of Mg–Al–carbonate hydrotalcite-like compounds,. *J. Mater. Chem.,* 2000, 10, 1713-1720.

[60] B. Subotic, A. Graovac, Kinetic analysis of autocatalytic nucleation during crystallization of zeolites, *Studies in Surface Science and Catalysis,* 1985, 24,199-206.